EurJIC
European Journal of Inorganic Chemistry

Research Article
doi.org/10.1002/ejic.202300478

Chemistry Europe
European Chemical Societies Publishing

www.eurjic.org

Special Collection

The Unique Ambiphilicity of Tellurium in the $[MesitylTe(I)(I_2)(I_3)]^-$ Anion

Vinícius Matos,[a] Ana Júlia Zimmermann Londero,[a] Maximilian Roca Jungfer,[b] Ulrich Abram,*[b] and Ernesto Schulz Lang*[a]

Dedicated to Prof. Roger Alberto on the occasion of his retirement and in recognition of more than 40 years of excellence in various fields of Inorganic Chemistry.

A first example of an aryltellurium(II) compound with three different bonding modes to iodine featuring covalent and non-covalent bonds such as two orthogonal, ambiphilic σ-hole interactions is introduced: $[MesTe(I)(I_2)(I_3)]^-$. It is a member of a series of mesityltellurenyl anions, which are formed during reactions of $(MesTe)_2$ with ZnI_2, phenanthroline (phen) and iodine. $[Zn(phen)_3][MesTe(I)_2]$ (**1**), $[Zn(phen)_3][\{MesTe(I)\text{-}(I)\ldots Te\text{-}(I)Mes\}\{MesTeI_2\}]$ (**2**) and $[Zn(phen)_3][MesTe(I)(I_2)(I_3)][MesTeI_2]$ (**3**) are isolated depending on the amount of iodine used. The products contain tellurium atoms bonded to a variety of iodine species (I^-, μ_2-I^-, I_2 and I_3^-) and are, thus, perfectly suitable to explore the amphiphilic behavior of tellurium(II) and its relevance for the formation of non-covalent bonds, where tellurium acts as both donor and acceptor simultaneously. The character of chalcogen and halogen bonds are evaluated by the combination of crystallographic data and computational methods.

Introduction

The interest in compounds with significant contributions of non-covalent interactions between atoms involving electrophilic regions in chalcogen and halogen centers has rapidly emerged in the recent years. The potential exploitation of their molecular and material properties is relevant for new applications in many fields.[1–8] Exemplarily, such compounds can be used as photoactive materials for electronic applications, as promoter of unusual redox processes,[9,10] or as potential catalysts.[11–17] This also involves representatives with (preferably) heavy chalcogens, which can establish non-covalent chalcogen-chalcogen and chalcogen-halogen interactions.[18]

Compounds containing electrophilic chalcogen atoms usually accept electrons through σ-holes. Such molecular regions with a positive electrostatic potential, which are located on the opposite side of one of the covalent bonds of e.g. tellurium, can be connected to a negatively polarized region of a donor atom resulting in a non-covalent interaction (Figure 1).[2]

In other words, non-covalent bonds can be formed by donor→σ*(E-R) interactions, in which the lone pair of a donor atom interacts with the antibonding σ* orbital of the heavy atom (E) and a more electronegative residue (R). The energy difference between the σ(E-R) and σ*(E-R) orbitals diminishes when going down the Periodic Table. Therefore, non-covalent bonds are stronger for tellurium compared to those of selenium or sulfur.[3,14,15] The exact nature of such σ-hole interactions is subject of discussion in numerous reviews and general considerations.[2–4,19–26] Figure 2 summarizes the main possibilities of donor→σ* interactions on the basis of the halogen and chalcogen bonding reported in the literature. To the best of our knowledge, examples of compounds in which different σ-hole-based bonding modes are established within the same molecule are not yet known for tellurium. Their study would be valuable and instructive for a deeper understanding of non-covalent bonding modes and allow a direct comparison of the individual contributions for the stabilization of such unusual compounds.

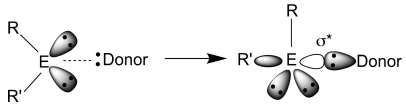

Figure 1. Presentation of a σ hole interaction. E = heavy chalcogen, R = alkyl or aryl and R′ = aryl, alkyl or halogen (F, Cl, Br, I).

[a] *V. Matos, A. J. Zimmermann Londero, Prof. Dr. E. Schulz Lang*
Universidade Federal de Santa Maria
Departamento de Química
97105-900, Santa Maria, Rio Grande do Sul (Brazil)
E-mail: eslang@ufsm.br
Homepage: http://www.ufsm.br/grupos/lmi

[b] *Dr. M. Roca Jungfer, Prof. Dr. U. Abram*
Institute of Chemistry and Biochemistry
Freie Universität Berlin
Fabeckstr. 34/36, 14195 Berlin (Germany)
E-mail: ulrich.abram@fu-berlin.de
Homepage: http://www.bcp.fu-berlin.de/chemie/chemie/forschung/InorgChem/agabram/index.html

Supporting information for this article is available on the WWW under https://doi.org/10.1002/ejic.202300478

This article is part of a joint Special Collection in honor of Roger Alberto.

Research Article
doi.org/10.1002/ejic.202300478

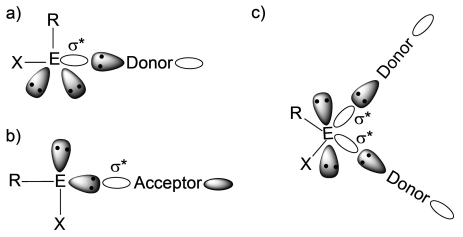

Figure 2. Schematic representation of the interactions of chalcogenyl units with donors or acceptors to generate antibonding σ* orbitals: a) chalcogenyl group interacting with an electron donor atom,[4,5,8] b) chalcogenyl group interacting with an electrophilic atom,[2,3,6,8] and c) chalcogenyl group interacting with two electron donors.[6,14] R = alkyl or aryl, and X = aryl, alkyl or halogen (F, Cl, Br, I).

Results and Discussion

As a part of our systematic studies about the reactivity of low-valent tellurium compounds, we performed reactions between dimesityl ditelluride, zinc iodide, phenanthroline and iodine. Different products are formed depending on the ratio of the reactants (Scheme 1). Stirring an equimolar mixture of the ditelluride, ZnI_2 and iodine in acetonitrile results in the precipitation of a red solid, which was identified as the $[Zn(phen)_3]^{2+}$ salt of diiodidomesityltelluride(II) (**1**). Single crystals of the product were obtained directly from the reaction mixture. The structure consists of isolated $[MesTeI_2]^-$ anions and $[Zn(phen)_3]^{2+}$ cations.[27] The Te–I bond lengths between 2.8736(5) and 3.0543(5) Å and the C–Te–I angles between 87.0(1) and 89.7(1)° are unexceptional and fall into the ranges, which were observed for other structures containing isolated $[MesTeI_2]^-$ ions.[28–32] An ellipsoid plot of the anion of compound **1** and more details about bond lengths and angles are given in Figure 3 and Table 1 together with the values of compound **2**, which is formed when a substoichiometric amount of ZnI_2 is used.

Decreasing the amount of ZnI_2 and, thus, limiting the formation of sufficient counterions for the formation of **1**, results in a partial aggregation of the tellurium species and the precipitation of a red solid of the composition $[Zn(phen)_3][\{MesTe(I)–(I)–Te(I)Mes\}\{MesTe(I)_2\}]$ (**2**). The formation of additional hydrolysis products with the water from phenanthroline hydrate became evident, particularly when these reactions were performed in undried acetonitrile. The accompanied decrease of the yields and purities could be avoided by the use of an acetic anhydride/methanol mixture as solvent.

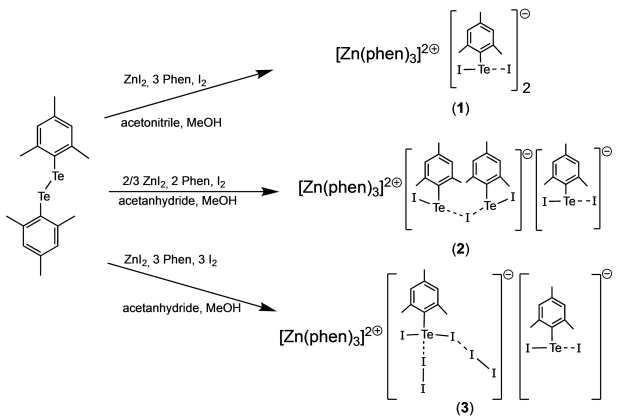

Scheme 1. Syntheses of the Te(II) compounds.

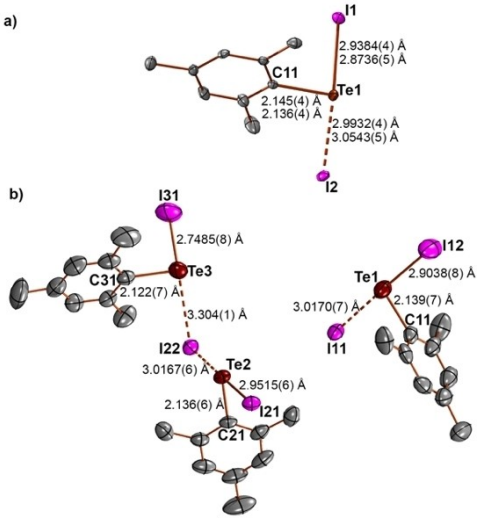

Figure 3. Structures of the anionic components of compounds **1** and **2**.

Table 1. Selected bond angles (°) in **1** and **2**.

Compound **1**[a]			
I1-Te1-I2	176.41(1), 176.75(1)	I1–Te1–C11	89.0(1), 89.7(1)
I2-Te1-C11	87.4(1), 87.0(1)		
Compound **2**			
I11–Te1–I12	177.85(3)	I11–Te1–C11	87.1(2)
I12–Te1–C11	91.9(2)	I21–Te2–I22	177.34(2)
I21–Te2–C21	95.4(2)	I22–Te2–C21	87.1(2)
I22–Te3–I31	168.0(2)	I22–Te3–C31	88.6(3)
I31–Te3–C31	92.8(2)	I22–Te3–I31	134.6(3)

[a] Values for two independent species.

Single crystals of **2** were obtained directly from the reaction mixture. The solid state structure consists of $[Zn(phen)_3]^{2+}$ cations and isolated $[MesTe(I)–(I)–Te(I)Mes]^-$ and $[MesTeI_2]^-$ anions (see Figure 3b). The formation of iodide bridges between aryl tellurium units is not common and the present case is only the second example for two tellurium(II) centers being connected by one iodide bridge. The I22–Te3–I31 angle of 134.6(3) is significantly bent, but roughly resembles the bonding features found for the previously published anion $[\{(2,6\text{–}Me_2Ph)Te(I)\}–(I)–\{Te(I)(2,6\text{-}Me_2PhTe)\}]^-$, in which also an intermediate Te–(I)–Te angle of 148.5° was established, while in the related mixed-valent Te(II)/Te(IV) compound $\{[(2,6\text{-}Me_2Ph)Te(I)\}–(I)–\{Te(I)_2(2,6\text{-}Me_2Ph)\}]$ the iodide bridge is almost linear with an Te-I–Te angle of 178.7°.[33] Much smaller Te–(I)–Te angles between 90.2 and 99.9° are found when two Te(IV)

Research Article
doi.org/10.1002/ejic.202300478

centers are bridged.[32,34–38] But it should be mentioned that only one of these examples contains a single iodide bridge.[32]

Having in mind the previously reported findings of Beckmann et al., that during the halogenation of diaryl ditellurides it is essential to control the stoichiometry and dynamic exchanges processes,[39] we used an excess of iodine in an additional experiment. And indeed, the treatment of a $(MesTe)_2/ZnI_2$/Phen mixture (1 : 1 : 3) with three equivalents of iodine results in the formation of a red solid, which contains a variety of iodine-based species. The composition of the product is best described as $[Zn(phen)_3][\{MesTe(I)_2\}][\{MesTe(I)(I_2)(I_3)\}]$ (**3**). Single crystals suitable for X-ray diffraction precipitated directly from the reaction mixture upon storing for several days in a refrigerator. Figure 4 depicts the solid state structure of the anion(s). Selected bond angles are summarized in Table 2.

Although weak I…I interactions between the two anions cannot be completely excluded in compound **3**, the treatment of the two tellurium-containing units as independent species seems to be appropriate. The I3C–I4 distance is as long as 3.75 Å and in none of the few examples with bridging tetraiodido species an iodine-iodine distance larger than 3.5 Å has been found.[40–47] This assumption is finally confirmed by a Hirshfeld analysis, which gave I…I interactions as weak as weak van der Waals contacts established between halogen atoms and aliphatic C–H bonds.

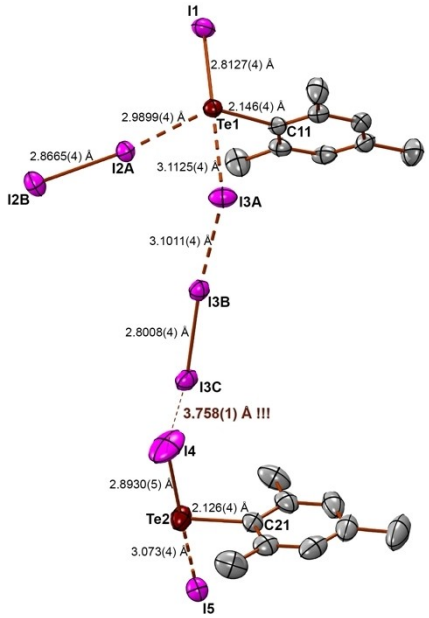

Figure 4. Structure of the anionic components of compound **3**. The dotted line between I3 C and I4 is topological and does not represent a bond.

Table 2. Selected bond angles (°) in compound **3**.

I1–Te1–I2A	93.01(1)	I1–Te1–I3A	179.72(1)
I1–Te1–C11	91.4(1)	I2A–Te1–I3A	86.81(1)
I2A–Te1–C11	117.9(1)	I3A–Te1–C11	88.5(1)
Te1–I2A–I2B	172.35(1)	Te1–I3A–I3B	114.71(1)
I3A–I3B–I3C	172.01(1)	I3B–I3C–I4	143.64(2)
I4–Te2–I5	176.54(2)	I4–Te2–C21	89.6(1)
I5–Te2–C21	90.9(1)		

Thus, the $[MesTe(I)(I_2)(I_3)]^-$ anion represents a unique species with a central heavy chalcogen atom being coordinated by three different halogen ligands, which makes it interesting to derive more information with regard to the bonding situation around tellurium, but also inside the iodine species. An inspection of the related tellurium-iodine bond lengths clearly shows three different values with the somewhat surprising result that the bond to the triiodide is the longest: ≈2.81 Å (I^-), ≈2.99 Å (I_2) and ≈3.11 Å (I_3^-). The iodine-iodine bonds of the coordinated I_2 species (≈2.87 Å) and inside the "iodine part" of the triiodido ligand (≈2.80 Å) are longer than in elemental iodine (2.715(6) Å).[48] Surprisingly, this can be interpreted as a significantly stronger donation of the aryltellurium(II) unit into the σ* orbital of I_2 compared to the much more delocalized situation found in the I_3^- moiety.

IR and Raman spectra of the compounds under study expectedly show resolved bands of the Te–I and I–I vibrations in the range between 120 and 200 cm^{-1}. A comparison of the spectra and a Table containing the experimental data is provided as Supporting Information (Figures S2.1 to S2.6). An unambiguous assignment of the bands, however, could not be made due to the complexity of the spectra resulting from the presence of multiple iodotellurenyl anions and the lack of similar compounds for comparison.[49–52]

The bonding of three different iodine species to one Te(II) center gives the extraordinary opportunity to study different covalent and non-covalent interactions in one single molecule. Thus, we performed some DFT calculations on the $[MesTe(I)(I_2)(I_3)]^-$ ion to learn more about the bonding situation within this molecule. The calculations were performed with a variety of functionals including B3LYP, B3LYP-D3, CAM-B3LYP, MP062X, PBE0-DH and MP2, all of which yield analogous descriptions. The obtained geometry of the B3LYP optimized using the triple ζ valence basis set with additional diffuse functions def2-TZVPD in the gas phase gives the best compromise between angular and distant accuracy. Results obtained with the other functionals show much larger angular deviations that outweigh the sometimes higher accuracies for the calculated distances. Overlays between the experimental and calculated structures for the regarded functionals (Figures S3.1.1 to S3.1.6) are shown in the Supporting Information, where also a Table with the differences between the experimental and calculated bonding parameters is deposited (Table S3.1.1). Main deviations (for all functionals) are found for the Te1–I2A of Figure 4 (the bond to the I_2 moiety), while main angular deviations are found for the Te1–I3A…I3B angle within the Te–I_3 moiety.

Figure 5 shows the electron localization function (ELF) mapping obtained with the B3LYP functional. Similar ELF maps are obtained with B3LYP-D3, CAM-B3LYP, M062X, PBE0-DH and MP2. They are shown as Figure S3.2.1 in the Supporting Information. Additionally, we added the ESP maps for all fragments to visualize the σ-holes involved in the discussed non-covalent interactions (Figures S3.2.2 to S3.2.8).

Research Article
doi.org/10.1002/ejic.202300478

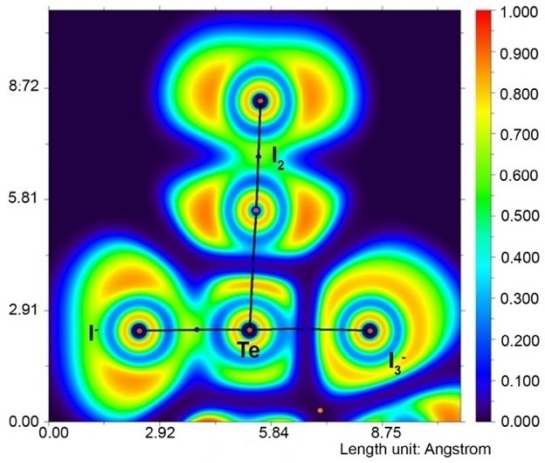

Figure 5. Electron localization function (ELF) mapping in the {I–Te(I)–I} plane of $[MesTeI(I_2)(I_3)]^-$ (B3LYP). Atomic (3,−3) critical points are brown, bond (3,−1) critical points are blue and ring (3,+1) critical points are orange. The paths resulting between (3,−3) and (3,−1) critical points are shown as thick black lines and correspond to bonds as defined by the quantum theory of atoms in molecules (QTAIM).

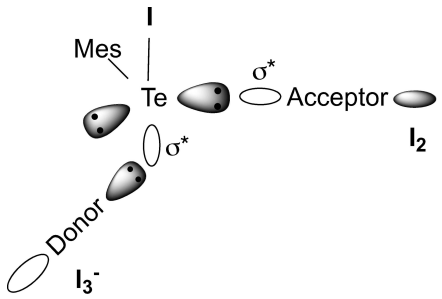

Figure 6. Schematic representation of the bonding situation in the $[MesTe(I)(I_2)(I_3)]^-$ anion.

It is obvious that the three iodine-tellurium bonds differ significantly. The monoiodide ligand shows features of a rather covalent bond (i.e. shared electron pair density between the contributing atoms). However, a distortion towards the iodide ion confirms the partially coordinative character of this bond. In comparison, the I_2 ligand is positioned linearly on a lone-pair of the tellurium atom, while it itself is electron-deficient along the bond axis. Consequently, this bond shows features of a halogen bond with the tellurium atom acting as donor into the anti-bonding σ*(I–I) orbital. Finally, the triiodido ligand coordinates to tellurium in *trans*-position to the monoiodido ligand. This bond, thus, shows characteristics of a potential chalcogen bond based on the absence of an electron pair on tellurium at the donating site of the I_3^- ligand. The s-character of the donor (in the case of the I_2 acceptor) iodine atoms increases from I_2 via I^- to I_3^-.

To further emphasize on these assumptions, we undertook topological analyses as well as an NBO analysis. Indeed, the second order perturbation analysis revealed energetically relevant donations in the suspected pattern: The iodide coordinates to tellurium building a covalent bond, while the tellurium atom acts as an electron pair donor to the σ-hole of the I_2 ligand (LP(Te)→σ*(I–I): ca. 31.5 kcal/mol) and as an electron pair acceptor with regard to two lone pairs of the triiodide iodine donor atom (LP(I)→σ*(Te–I): ca. 22.5 kcal/mol & LP(I)→σ*(Te–I): ca. 23.1 kcal/mol) establishing a chalcogen bond, see Figure 6. The bond between the triiodides donor atom and the corresponding I_2 moiety inside of the triiodide is consistent with a halogen bond (LP(I)→σ*(I–I): ca. 11.3 kcal/mol & LP(I)→σ*(I–I): ca. 21.5 kcal/mol) and again involves two of the iodide moieties lone pairs. The summary of relevant contributions in the NBO analysis is given in the Supporting Information.

Further support for the bonding situation depicted in Figure 6 is given by the results of an energy decomposition analysis (EDA), which has been performed for several functionals (see Supporting Information). Expectedly and in accord with the previous methods, the results show, that all Te–I and I–I interactions are considerably orbital controlled. Electrostatic interactions also play a significant role, while dispersion is nearly neglectable. The tellurium-iodide bond (Te1–I1 in Figure 4) is much more orbital-governed (covalent) compared to the other Te–I bonds, which are similar to the bond between I^- and I_2 in the I_3^- anion.

A reduced gradient analysis (RDG) confirms the presence of weak non-covalent interactions between tellurium and I_3^- or I_2 as well as within the I_3^- moiety. The graphical RDG analysis is shown in Figure 7.

We located a (3,−1) critical bond along the bond axes of the atoms involved in these interactions. The properties of the electron density at the bond critical points further support the

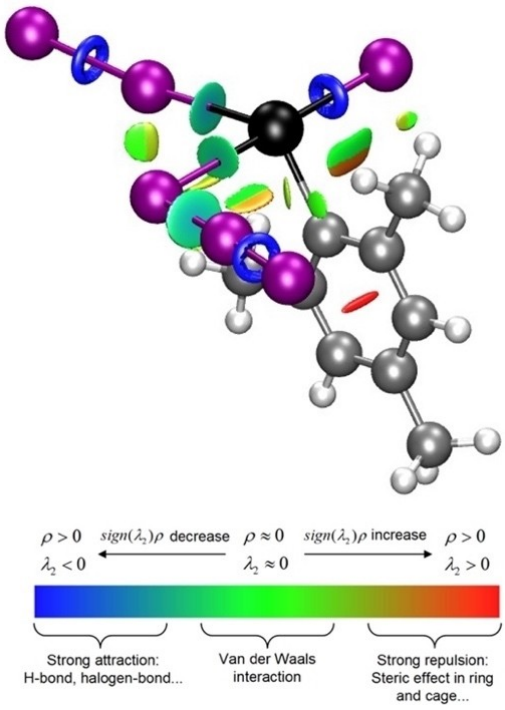

Figure 7. Reduced density gradient (RDG) analysis for the visualization of weak interactions.[53]

Research Article
doi.org/10.1002/ejic.202300478

findings according to the quantum theory of atoms in molecules (QTAIM). They allow an evaluation of the closed- or shared-shell nature of bonds based on the electron density at the bond critical point ρ_b, the Laplacian $\triangle^2\rho_b$, eigenvalues of the Hessian matrix λ_1, λ_2 and λ_3 and the ellipticity ε.[54–57] The criteria applied for the classification of the corresponding interactions are explained in detail in the Supporting Information. For the $[MesTe(I)(I_2)(I_3)]^-$ anion under study following information could be derived: (i) only the bond critical point on the Te–C bond can be understood as a polar covalent bond, (ii) the bonds between I^- and tellurium are similar to the covalent I–I bonds in both the triiodide as well as the iodine moieties. They can be classified as non-polar, covalent bonds, (iii) the bonds between tellurium and I_3^- and I_2 as well as the bond between the iodide and the iodine inside of the triiodide moiety are consistent with polar, non-covalent closed-shell interactions and (iv) a large ellipticity emphasizes surprisingly significant π-components in the bond between tellurium and I^- and I_3^-.

Since the overall analysis of such systems may be tedious when calculating all the above properties, we checked the feasibility of some simple functions along the bonds between the atoms involved to provide an easier way to distinguish the different bonding types (i.e. to identify the donor and the acceptor behavior in such cases). For this, we calculated the orbital overlap distance functions as well as the localized orbital locator (LOL) functions between the two respective atoms. Both functions gave specific profiles for covalent bonds as well as the non-covalent interactions discussed above. A superposition of the respective graphs is shown in the Supporting Information (Figures S3.3.2 and S3.2.3). It also contains a more detailed explanation of the criteria for the assignment. It becomes obvious that a characteristic profile of these function along the bond corresponds to each type of bonds, which is well suitable for a classification of the donor/acceptor contributions of atoms to covalent and non-covalent bonds. For the present case, the results support a bonding situation in $[MesTe(I)(I_2)(I_3)]^-$ as is depicted in Figure 6.

Conclusions

The tellurium(II) species of this study exemplifies the interactions of tellurium(II) with different iodine species (I^-, μ_2-I^-, I_2 and I_3^-). Different types of σ-hole interactions within a single atom of a single site within a single molecule were detected for the first time for a tellurium atom in the $[MesTe(I)(I_2)(I_3)]^-$ anion. They are characterized by X-ray crystallography combined with an analysis of the electronic bond properties derived from DFT calculations.

Experimental Section

All chemicals were purchased commercially and used without further purification. Solvents were dried by standard methods. $(MesTe)_2$ was prepared according to literature procedures.[58]

Elemental analyses were determined with a Heraeus Vario El III elemental analyzer. FTIR spectra were recorded in a Bruker Vertex spectrometer using attenuated total reflection (ATR). Confocal FT-Raman spectra between 3600 and 60 cm^{-1} were performed with a Bruker Senterra micro-Raman spectrometer using a 785 nm laser. ^{125}Te NMR spectra were recorded in DMSO on a Bruker-Avance III 600 MHz spectrometer. Me_2Te was used as external standard.

Crystallography

The X-ray data were collected on a Bruker D8 Venture diffractometer equipped with a Photon 100 detector, an Incoatec micro focusing Montel optic X-ray tube with $Mo_{K\alpha}$ radiation (λ = 0.71073 Å), and an Oxford Cryostream 900 temperature unit operating at 100 K. The structures were solved by direct methods using SHELXT and refined with SHELXL on F^2 using anisotropic temperature parameters for all non-hydrogen atoms.[59,60] Hydrogen atoms positions were calculated for idealized positions using the riding-model option of SHELXL. All crystallographic illustrations are original and were drawn with DIAMOND.[61]

Syntheses

$[Zn(phen)_3][MesTe(I)_2]_2 \cdot CH_3CN$ (**1**). $(MesTe)_2$ (49.7 mg, 0.1 mmol) was added to a mixture of ZnI_2 (31.9 mg, 0.1 mmol) and phenanthroline hydrate (59.4 mg, 0.3 mmol) dissolved in 10 mL of CH_3CN/CH_3OH (1:1). The mixture was stirred at room temperature for 10 min. During this time, solid I_2 (25.3 mg, 0.1 mmol) was added in small portions. After an additional stirring for 5 min., the red precipitate was filtered off, washed with CH_3OH and dried. Red single crystals formed from the mother liquor within three days. Spectroscopic data (IR, Raman) and elemental analyses confirmed the identity of both the precipitate and crystals as **1**. Yield: 113.9 mg (69%). Elemental analysis: Calcd for $C_{56}H_{48}I_4N_7Te_2Zn$: C, 40.36; H, 2.89; N, 5.23%; Found: C, 40.01; H, 2.86; N, 5.29%. IR: $\tilde{\nu}$ = 3050 (w), 2962 (w), 2904 (w), 1623 (w), 1579 (w), 1514 (m), 1423 (m), 1140 (m), 1101 (m), 841 (s), 768 (m), 722 (s), 641 (m), 541 (m), 420 (m), 324 (m), 286 (m), 241 (m), 193 (s), 130 cm^{-1} (s). Raman: $\tilde{\nu}$ = 132 (s), 109 cm^{-1} (s). ^{125}Te NMR (DMSO): δ = −589 ppm.

$Zn(phen)_3][MesTe(I)–(I)–Te(I)Mes][MesTe(I)_2]$ (**2**). $(MesTe)_2$ (74.6 mg, 0.15 mmol) was added to a mixture of ZnI_2 (31.9 mg, 0.1 mmol) and phenanthroline hydrate (59.4 mg, 0.3 mmol) dissolved in 10 mL of $CH_3CO_2COCH_3/CH_3OH$ (1:1). The mixture was stirred for 10 min at room temperature and solid I_2 (38 mg, 0.15 mmol) was added in small portions. A red precipitate formed, which was filtered off after stirring for an additional 5 min. and washed with CH_3OH. A crystalline material of the same compound deposited within three days from the mother liquor. Spectroscopic data (IR, Raman) and elemental analyses confirmed the homogeneity and thus identity of both the precipitate and crystals as **2**. Yield: 123.1 mg (62%). Elemental analysis: Calcd for $C_{63}H_{57}I_5N_6Te_3Zn$: C, 38.20; H, 2.90; N, 4.24%; Found: C, 38.58; H, 2.95; N, 4.38%. IR: $\tilde{\nu}$ = 3050 (w), 2962 (w), 2904 (w), 1623 (w), 1579 (w), 1514 (m), 1423 (m), 1140 (m), 1101 (m), 841 (s), 768 (m), 722 (s), 641 (m), 541 (m), 420 (m), 324 (m), 286 (m), 241 (m), 193 (s), 130 cm^{-1} (s). Raman: $\tilde{\nu}$ = 136 (s), 105 (s), 63 cm^{-1} (s). ^{125}Te NMR (DMSO): δ = −589 ($[MesTeI_2]^-$), −257 ppm ($[MesTe(I)–I–Te(I)Mes]^-$).

$[Zn(phen)_3][MesTe(I)(I_2)(I_3)][MesTe(I)_2]$ (**3**). $(MesTe)_2$ (49.7 mg, 0.1 mmol) was added to a mixture of ZnI_2 (31.9 mg, 0.1 mmol) and phenantroline hydrate (59.4 mg, 0.3 mmol) dissolved in 10 mL of $CH_3CO_2COCH_3/CH_3OH$ (1:1). The mixture was stirred for 10 min at room temperature and solid I_2 (76.1 mg, 0.3 mmol) was added in small portions during this time. After an additional stirring for 5 min., the red precipitate formed was filtered off and washed with

Research Article
doi.org/10.1002/ejic.202300478

methanol. A crystalline material could be obtained from the mother liquor by leaving it for three days at room temperature. Spectroscopic data (IR, Raman) and elemental analyses confirmed the homogeneity and thus identity of both the precipitate and crystals as **3**. The low solubility of the product even in DMSO prevented from the measurement of a ^{125}Te NMR spectrum of reasonable quality (only the signal of the $[MesTe(I)_2]^-$ anion could be detected with low intensity). Yield: 120.6 mg (57%). Elemental analysis: Calcd for $C_{54}H_{46}I_8N_6Te_2Zn$: C, 30.67; H, 2.19; N, 3.97%; Found: C, 30.72; H, 2.19; N, 3.97%. IR: $\tilde{\nu}$ = 3050 (w), 2962 (w), 2904 (w), 1623 (w), 1579 (w), 1514 (m), 1423 (m), 1140 (m), 1101 (m), 841 (s), 768 (m), 722 (s), 641 (m), 541 (m), 420 (m), 324 (m), 286 (m), 241 (m), 193 (s), 130 cm^{-1} (s). Raman: $\tilde{\nu}$ = 156 (s), 141 (w), 128 (s), 83 cm^{-1} (s). ^{125}Te NMR (DMSO): δ = −595 ppm.

Computational chemistry

DFT and MP2 calculations were performed on the high-performance computing systems of the Freie Universität Berlin ZEDAT (Curta)[62] using the program package GAUSSIAN 16.[63] The gas phase geometry optimization was performed using coordinates derived from the X-ray crystal structure using GAUSSVIEW.[64] The calculations were performed with the hybrid density functional B3LYP, the dispersion (Grimme D3) corrected variant B3LYP-D3, the long-range corrected variant CAM-B3LYP, the Minnesota hybrid density functional M062X, the double hybrid functional PBE0-DH and Møller-Plesset second-order perturbation theory (MP2).[65–71] The triple-ζ relativistic pseudopotential def2-TZVPD basis set was applied to all atoms including the respective effective core potential (ECP) for Te and I.[72–74] All basis sets as well as the ECPs were obtained from the basis set exchange database.[75] Frequency calculations after the optimizations confirmed the convergence and no negative frequencies were obtained. Further analysis of the obtained wave-functions was performed with the free multifunctional wavefunction analyzer Multiwfn.[76] The reduced density gradient (RDG) method was used as implemented in Multiwfn and visualized using the VMD package.[77,78] The Hirshfeld analysis on the solid-state structure of of $[Zn(bpy)_3][MesTe(I)(I_2)(I_3)][MesTe(I)_2]$ was used as implemented in Multiwfn and visualized using the VMD package.[77,78] Overlays of the experimental and calculated structures were superimposed using Mercury.[79] The results of all functionals indicate similar trends and numeric values.

Supporting Information

The authors have cited references within the Supporting Information.[54–57,74–77]

Acknowledgements

This work was supported by the Coordenadoria de Aperfeiçoamento de Pessoas de Nível Superior (CAPES/DAAD – Probral n. 88881.144118/2017 and CAPES/PRINT, n. 88881.310412/2018, Brazil), Conselho Nacional de Desenvolvimento Científico e Tecnológico (CNPq) and German Academic Exchange Service (DAAD, Germany). We gratefully acknowledge the High-Performance-Computing (HPC) Centre of the Zentraleinrichtung für Datenverarbeitung (ZEDAT) of the Freie Universität Berlin for computational time and support. Open Access funding enabled and organized by Projekt DEAL.

Conflict of Interests

The authors declare no conflict of interest.

Data Availability Statement

The data that support the findings of this study are available in the supplementary material of this article.

Keywords: density functional calculations · iodides · non-covalent bonds · sigma holes · tellurium

[1] M. H. Kolár, P. Hobza, *Chem. Rev.* **2016**, *116*, 5155–5187.
[2] L. Vogel, P. Wonner, S. M. Huber, *Angew. Chem. Int. Ed.* **2019**, *58*, 1880–1891.
[3] G. Haberhauer, R. Gleiter, *Angew. Chem. Int. Ed.* **2020**, *59*, 21236–21243.
[4] M. C. Aragoni, M. Arca, F. A. Devillanova, A. Garau, F. Isaia, V. Lippolis, A. Mancini, *Bioinorg. Chem. Appl.* **2007**, 1–46.
[5] A. Mohajeri, A. H. Pakiari, N. Bagheri, *Chem. Phys. Lett.* **2009**, *467*, 393–397.
[6] V. Oliveira, D. Cremer, E. Kraka, *J. Phys. Chem. A* **2017**, *121*, 6845–686.
[7] V. Kumar, Y. Xu, D. L. Bryce, *Chem. Eur. J.* **2020**, *26*, 3275–3286.
[8] A. J. Z. Londero, N. R. Pineda, V. Matos, P. C. Piquini, U. Abram, E. S. Lang, *J. Organomet. Chem.* **2020**, *929*, 121553.
[9] S. M. Godfrey, N. Ho, C. A. McAuliffe, R. G. Pritchard, *Angew. Chem. Int. Ed.* **1996**, *35*, 2344–2346.
[10] C. N. Cechin, G. F. Razera, B. Tirloni, P. C. Piquini, L. M. de Carvalho, U. Abram, E. S. Lang, *Inorg. Chem. Commun.* **2020**, *118*, 107966.
[11] A. V. Novikov, A. N. Usoltsev, S. A. Adonin, A. A. Bardin, D. G. Samsonenko, G. V. Shilov, M. N. Sokolov, K. J. Stevenson, S. M. Aldoshin, V. P. Fedinc, P. A. Troshin, *J. Mater. Chem. A* **2020**, *8*, 21988–21992.
[12] P. C. Ho, J. Z. Wang, F. Meloni, I. Vargas-Baca, *Coord. Chem. Rev.* **2020**, *422*, 213464.
[13] A. F. Cozzolino, P. J. W. Elder, I. Vargas-Baca, *Coord. Chem. Rev.* **2011**, *255*, 11–12.
[14] T. Chivers, R. S. Laitinen, *Chem. Soc. Rev.* **2015**, *44*, pp. 1725–1739.
[15] S. Benz, A. I. Poblador-Bahamonde, N. Low-Ders, S. Matile, *Angew. Chem. Int. Ed.* **2018**, *57*, 5408–5412.
[16] J. Bamberger, F. Ostler, O. G. Mancheño, *ChemCatChem* **2019**, *11*, 5198–5211.
[17] M. Breugst, J. J. Koenig, *Eur. J. Org. Chem.* **2020**, 5473–5487.
[18] V. Lippolis, F. Isaia, *Charge-Transfer (C.-T.) Adducts and Related Compounds, in: Handbook of Chalcogen Chemistry: New Perspectives in Sulfur, Selenium and Tellurium* (Eds.: F. A. Devillanova), RSC, **2007**, pp. 477–446.
[19] C. B. Aakeroy, D. L. Bryce, G. R. Desiraju, A. Frontera, A. C. Legon, F. Nicotra, K. Rissanen, S. Scheiner, G. Terraneo, P. Metrangolo, G. Resnati, *Pure Appl. Chem.* **2019**, *91*, 1889–1892.
[20] P. Politzer, J. S. Muttay, T. Clark, *Phys. Chem. Chem. Phys.* **2013**, *15*, 11178–11189.
[21] C. Aragoni, Y. Torubaev, *Structural Features of Chalcogen Bonds and Weak Interactions Involving Chalcogens, in: Chalcogen Chemistry: Fundamentals and Applications* (Eds.: V. Lippolis, C. Santi, E. J. Leonardo, A. L. Braga), RSC, **2023**, pp. 435–475.
[22] M. Arca, G. Ciancaleoni, A. Pintus, *Computational Methods to Study Chalcogen Bonds in: Chalcogen Chemistry: Fundamentals and Applications* (Eds.: V. Lippolis, C. Santi, E. J. Leonardo, A. L. Braga), RSC, **2023**, pp. 476–493.
[23] M. C. Aragoni, M. Arca, V. Lippolis, A. Pintus, Y. Torubaev, E. Podda, *Molecules* **2023**, *28*, 3133.
[24] P. Scilabra, G. Terraneo, G. Resnati, *Acc. Chem. Res.* **2019**, *52*, 1313–1324.
[25] M. A. A. Ibrahim, E. M. Z. Telb, *ACS Omega* **2020**, *5*, 21631–21640.
[26] M. C. Aragoni, M. Arca, C. Caltagirone, C. Castellano, F. Demartin, P. G. Jones, T. Pivetta, E. Podda, V. Lippolis, S. Murgia, G. Picci, *J. Org. Chem.* **2022**, *87*, 15448–15465.
[27] Deposition Numbers 2242884 (for **1**), 2086400 (for **2**), and 2086401 (for **3**) contain the supplementary crystallographic data for this paper. These data are provided free of charge by the joint Cambridge Crystallographic Data Centre and Fachinformationszentrum Karlsruhe Access Structures service.

[28] M. C. Aragoni, M. Arca, A. J. Blake, E. Cadoni, L. O. Copolovici, F. Isaia, V. Lippolis, S. Murgia, A. M. Pop, C. Silvestru, J. P. Tidey, R. A. Varga, *New J. Chem.* **2019**, *43*,11821–11831.
[29] P. G. Jones, C. G. Hrib, W.-W. du Mont, *CSD, Private Communication*, **2015**, DOXHIJ.
[30] P. G. Jones, R. Brzoi, W.-W. du Mont, N. Schulze, *CSD, Private Communication*, **2015**, SUGCUU.
[31] G. M. de Oliveira, E. Faoro, E. S. Lang, G. A. Casagrande, *Z. Anorg. Allg. Chem.* **2006**, *632*, 659–663.
[32] E. Faoro, G. M. de Oliveira, E. S. Lang, *J. Organomet. Chem.* **2006**, *691*, 5867–5872.
[33] E. Faoro, G. M. de Oliveira, E. S. Lang, *J. Organomet. Chem.* **2009**, *694*, 1557–1561.
[34] N. W. Alcock, W. D. Harrison, *J. Chem. Soc. Dalton Trans.* **1984**, 869875.
[35] P. H. Bird, V. Kumar, B. C. Pant, *Inorg. Chem.* **1980**, *19*, 2487–2492.
[36] C. G. Hrib, J. Jeske, P. G. Jones, W.-W. du Mont, *Dalton Trans.* **2007**, 3483–3485.
[37] Y. V. Torubaev, A. A. Pasynsky, I. V. Skabitsky, *Russ. J. Coord. Chem.* **2009**, *35*, 341–246.
[38] N. Kuhn, T. Kratz, G. Henkel, *Z. Naturforsch. B* **1996**, *51*, 295–297.
[39] J. Beckmann, M. Hesse, H. Poleschner, K. Seppelt, *Angew. Chem. Int. Ed.* **2007**, *46*, pp. 8277–8280.
[40] R. Gray, D. J. Gulliver, W. Levason, M. Webster, *Inorg. Chem.* **1983**, *22*, 2362–2366.
[41] P. H. Svensson, J. Rosdahl, L. Kloo, *Chem. Eur. J.* **1999**, *5*, 305–311.
[42] P. H. Svensson, L. Kloo, *Inorg. Chem.* **1999**, *38*, 3390–3393.
[43] M. F. Belicchi, G. G. Fava, C. Pelizzi, *Acta Crystallogr. Sect. B* **1981**, *37*, 924–926.
[44] N. Masuhara, S. Nakashima, K. Yamada, *Chem. Lett.* **2005**, *34*, 1352–1353.
[45] J. Le Bras, H. Amouri, J. Vaissermann, *Inorg. Chem.* **1998**, *37*, 5056–5060.
[46] L. Hewison, S. H. Crook, B. E. Mann, A. J. H. M. Meijer, H. Adams, P. Sawle, R. A. Motterlini, *Organometallics* **2012**, *31*, 5823–5834.
[47] X. Jin, K. Tang, W. Liu, Y. Tang, *Heteroat. Chem.* **1995**, *6*, 41–43.
[48] F. van Bolhuis, P. B. Koster, T. Migchelsen, *Acta Crystallogr.* **1967**, *23*, 90–91.
[49] W. R. McWhinnie, M. G. Patel, *J. Chem. Soc. Dalton Trans.* **1972**, 199–202.
[50] W. R. McWhinnie, P. Thavornyutikarn, *J. Chem. Soc. Dalton Trans.* **1972**, 551–554.
[51] J. M. Alía, H. G. M. Edwards, F. J. Garcia-Navarro, *J. Mol. Struct.* **1999**, *508*, 51–58.
[52] P. C. Srivastava, S. Bajpai, R. Lath, R. Kumar, V. Singh, S. Dwivedi, T. J. Butcher, S. Hayashi, W. Nakanishi, *Polyhedron* **2008**, *27*, 835–848.
[53] E. R. Johnson, S. Keinan, P. Mori-Sánchez, J. Contreras-García, A. J. Cohen, W. Yang, *J. Am. Chem. Soc.* **2010**, *132*, 6498–6506.
[54] R. Hilal, S. G. Aziz, A. O. Alyoubi, S. Elroby, *Procedia Comput. Sci.* **2015**, *51*, 1872–1877.
[55] W. Wang, B. Ji, Y. Zhang, *J. Phys. Chem. A* **2009**, *113*, 8132–8135.
[56] R. F. W. Bader, *Atoms in Molecules: A Quantum Theory*, Clarendon, Oxford, UK, **1990**.
[57] C. S. López, A. R. de Lera, *Curr. Org. Chem.* **2011**, *15*, 3576–3593.
[58] H. J. Reich, M. L. Cohen, P. S. Clark, *Org. Synth.* **1979**, *59*, 141–142.
[59] G. M. Sheldrick, *Acta Crystallogr. Sect. A* **2008**, *64*, 112–122.
[60] G. M. Sheldrick, *Acta Crystallogr. Sect. C* **2015**, *71*, 3–8.
[61] H. Putz, K. Brandenburg, DIAMOND, Crystal and Molecular Structure Visualization Crystal Impact; GbR: Bonn, Germany, version 4.6.5, **2021**.
[62] High performance computing (HPC) system Curta at Freie Universität Berlin. DOI: 10.17169/refubium-26754.
[63] Gaussian 16, Revision A.02, M. J. Frisch, G. W. Trucks, H. B. Schlegel, G. E. Scuseria, M. A. Robb, J. R. Cheeseman, G. Scalmani, V. Barone, G. A. Petersson, H. Nakatsuji, X. Li, M. Caricato, A. V. Marenich, J. Bloino, B. G. Janesko, R. Gomperts, B. Mennucci, H. P. Hratchian, J. V. Ortiz, A. F. Izmaylov, J. L. Sonnenberg, D. Williams-Young, F. Ding, F. Lipparini, F. Egidi, J. Goings, B. Peng, A. Petrone, T. Henderson, D. Ranasinghe, V. G. Zakrzewski, J. Gao, N. Rega, G. Zheng, W. Liang, M. Hada, M. Ehara, K. Toyota, R. Fukuda, J. Hasegawa, M. Ishida, T. Nakajima, Y. Honda, O. Kitao, H. Nakai, T. Vreven, K. Throssell, J. A. Montgomery Jr., J. E. Peralta, F. Ogliaro, M. J. Bearpark, J. J. Heyd, E. N. Brothers, K. N. Kudin, V. N. Staroverov, T. A. Keith, R. Kobayashi, J. Normand, K. Raghavachari, A. P. Rendell, J. C. Burant, S. S. Iyengar, J. Tomasi, M. Cossi, J. M. Millam, M. Klene, C. Adamo, R. Cammi, J. W. Ochterski, R. L. Martin, K. Morokuma, O. Farkas, J. B. Foresman, D. J. Fox, Gaussian, Inc., Wallingford CT, **2016**.
[64] R. Dennington, T. A. Keith, J. M. Millam, GaussView, Version 6, Semichem Inc., Shawnee Mission, KS, **2016**.
[65] S. H. Vosko, L. Wilk, M. Nusair, *Can. J. Phys.* **1980**, *58*, 1200–1211.
[66] A. D. Becke, *J. Chem. Phys.* **1993**, *98*, 5648–5652.
[67] C. Lee, W. Yang, R. G. Parr, *Phys. Rev. B* **1988**, *37*, 785–789.
[68] S. Grimme, *J. Comput. Chem.* **2004**, *25*, 1463–1473.
[69] T. Yanai, D. P. Tew, N. C. Handy, *Chem. Phys. Lett.* **2004**, *393*, 51–57.
[70] Y. Zhao, D. G. Truhlar, *Theor. Chem. Acc.* **2008**, *120*, 215–241.
[71] E. Brémond, C. Adamo, *J. Chem. Phys.* **2011**, *135*, 024106.
[72] K. A. Peterson, D. Figgen, E. Goll, H. Stoll, M. Dolg, *J. Chem. Phys.* **2003**, *119*, 11113–11123.
[73] D. Rappoport, F. Furche, *J. Chem. Phys.* **2010**, *133*, 134105.
[74] F. Weigend, R. Ahlrichs, *Phys. Chem. Chem. Phys.* **2005**, *7*, 3297.
[75] K. L. Schuchardt, B. T. Didier, T. Elsethagen, L. Sun, V. Gurumoorthi, J. Chase, J. Li, T. L. Windus, *J. Chem. Inf. Model.* **2007**, *47*, 1045–1052.
[76] T. Lu, F. Chen, *J. Comput. Chem.* **2012**, *33*, 580–592.
[77] E. R. Johnson, S. Keinan, P. Mori-Sánchez, J. Contreras-García, A. J. Cohen, W. Yang, *J. Am. Chem. Soc.* **2010**, *132*, 6498–6506.
[78] W. Humphrey, A. Dalke, K. Schulten, *J. Mol. Graphics* **1996**, *14*, 33–38.
[79] C. F. Macrae, I. Sovago, S. J. Cottrell, P. T. A. Galek, P. McCabe, E. Pidcock, M. Platings, G. P. Shields, J. S. Stevens, M. Towler, P. A. Wood, *J. Appl. Crystallogr.* **2020**, *53*, 226–235.

Manuscript received: July 28, 2023
Revised manuscript received: August 7, 2023
Accepted manuscript online: August 8, 2023
Version of record online: August 31, 2023